Exact quantum states for the diagonal Bianchi type IX model with negative cosmological constant

Robert Paternoga and Robert Graham

Fachbereich Physik, Universität-Gesamthochschule Essen, 45117 Essen, Germany

(Received 20 May 1996)

Quantum states of the diagonal Bianchi type IX model with *negative* cosmological constant Λ are obtained by transforming the Chern-Simons solution in Ashtekar's variables to the metric representation. We apply our method developed earlier for $\Lambda > 0$ and obtain five linearly independent solutions by using the complete set of topologically inequivalent integration contours in the required generalized Fourier transformation. A caustic in minisuperspace separates two Euclidean regimes at *small* and *large* values of the scale parameter from a single classically interpretable Lorentzian regime in between, corresponding to the fact that classically these model universes recollapse. Just one particular solution out of the five we find gives a normalizable probability distribution on both branches of the caustic. However, in contrast with the case of positive cosmological constant, this particular solution neither satisfies the semiclassical no-boundary condition, nor does the special initial condition it picks out for $\hbar \to 0$ evolve into a classically interpretable universe. [S0556-2821(96)04120-3]

I. INTRODUCTION

Quantum gravity with a nonvanishing cosmological constant formulated in Ashtekar's spin-connection variables [1–5] has interesting physical states given by the exponential of the Chern-Simons functional [5–7] and appropriate transformations thereof. In order to elucidate the physical meaning of such states it is interesting to consider their restrictions to spatially homogeneous cosmological models. In a recent paper [8], henceforth quoted as [I], we considered the diagonal Bianchi type IX models with positive cosmological constant from this point of view and found that five linearly independent, physical states in the metric representation could be derived from the Chern-Simons functional. This set of solutions was found to be in one-to-one correspondence with the set of topologically different integration contours which exist for the generalized Fourier transformation from the Ashtekar representation to the metric representation. Because of the positivity of the cosmological constant the quantum states found in [I] describe an expanding (or collapsing), classically interpretable, Lorentzian universe at large scale parameters. On the other hand, at sufficiently small scale parameters the action defined by the exponent of the wave function becomes imaginary and can be associated only with a quantum-mechanically allowed Euclidean universe. The two "phases" are separated by a caustic surface in minisuperspace. It was found that only one of the five linearly independent states defines a normalizable probability distribution on this caustic, that this state satisfies the no-boundary condition of Hartle and Hawking [9,10] semiclassically for $\hbar \to 0$ (which means on scales large compared to the Planck scale), and that, again for $\hbar \to 0$, it picks out an initial condition which evolves into a classically interpretable Lorentzian universe. For details and further literature we refer to [I].

It is now of interest to consider also what happens for negative cosmological constant, even though it seems very unlikely that our Universe has $\Lambda < 0$. (The age problem resulting from recently measured high values of the Hubble parameter [11] and the measured large age of globular star clusters and also the observed high density of galaxies with large redshifts seem to call for $\Lambda > 0$.) Our motivation is rather to try the method of [I] for a model universe which recollapses, i.e., for which quantum-mechanically a classically interpretable Lorentzian evolution phase is bounded for small *and* large values of the scale parameter by Euclidean evolution phases. Therefore, we have to expect the appearance of two caustic surfaces in the minisuperspace of these models, one at small and the other at large scale parameter. Is there still a wave function, or are there even several, which give a normalizable probability distribution on these surfaces, and how are these wave functions related to the no-boundary state?

To answer these questions we apply in Sec. II the method of [I] to obtain expressions again for five linearly independent physical states and identify the caustic surfaces in minisuperspace. In Sec. III we determine the behavior of the absolute square of the wave functions on the caustic and identify a single physical state which gives a normalizable probability distribution in this way. In Sec. IV we summarize our results. Within the narrow class of models we consider here, they seem to rule out, with high probability, a classically evolving universe with $\Lambda < 0$.

II. QUANTUM STATES GENERATED BY THE CHERN-SIMONS SOLUTION

In this section we want to construct solutions of the Wheeler-DeWitt equation for the diagonal Bianchi type IX model with a cosmological constant $\Lambda < 0$:

$$\begin{aligned}
\{[\hbar \partial_\alpha - \Phi_{,\alpha}][\hbar \partial_\alpha + \Phi_{,\alpha}] - [\hbar \partial_+ - \Phi_{,+}][\hbar \partial_+ + \Phi_{,+}] \\
- [\hbar \partial_- - \Phi_{,-}][\hbar \partial_- + \Phi_{,-}] \\
+ 3(8\pi)^2 \Lambda e^{6\alpha}\} \Psi(\alpha, \beta_\pm; \Lambda) = 0 ,
\end{aligned} \tag{2.1}$$

where

$$\Phi := 2\pi e^{2\alpha}\,\mathrm{Tr}e^{2\beta} \quad \text{and}$$

$$\boldsymbol{\beta} = (\beta_{ij}) := \mathrm{diag}(\beta_+ + \sqrt{3}\beta_-, \beta_+ - \sqrt{3}\beta_-, -2\beta_+). \tag{2.2}$$

In this notation ∂_+ and ∂_- denote derivatives with respect to the variables β_+ and β_-, respectively. By writing the Wheeler-DeWitt equation in the form (2.1) we have assumed a specific factor ordering, which is suggested by a supersymmetric extension of the model [12–14]. A different factor ordering is obtained by considering Eq. (2.1) with Φ replaced by $-\Phi$. In the present paper, as in [I], we will restrict ourselves to the factor ordering as in Eq. (2.1), while a brief comment on the solutions in the second case $\Phi \rightarrow -\Phi$ is given in the Appendix.

If the expression (2.2) for Φ is inserted into the Wheeler-DeWitt equation (2.1), the following more explicit form is obtained:

$$\left\{ \frac{\hbar^2}{3\pi^2}\left[\frac{\partial^2}{\partial\alpha^2} - \frac{\partial^2}{\partial\beta_+^2} - \frac{\partial^2}{\partial\beta_-^2}\right] - \frac{2\hbar}{\pi}a^2\,\mathrm{Tr}e^{2\boldsymbol{\beta}} \right.$$

$$\left. + a^4\,\mathrm{Tr}(e^{4\boldsymbol{\beta}} - 2\,e^{-2\boldsymbol{\beta}}) + \Lambda a^6 \right\} \Psi(\alpha, \beta_\pm; \Lambda) = 0, \tag{2.3}$$

where we have introduced the mean scale factor $a := 2\,e^{\alpha}$. As in the case $\Lambda > 0$, solutions of Eq. (2.3) can be obtained by a transformation to the Ashtekar representation, where the Chern-Simons functional, restricted to the Bianchi type IX case, turns out to be an exact solution. Two of the Fourier integrals which occur in the transformation back to the metric representation can be carried out analytically without any loss of generality and afterwards the same one-dimensional integral representation as in [I] is obtained:[1]

$$\Psi(\kappa, \beta_\pm; \lambda) \propto \int_{\mathcal{C}} du\,\exp\left[\frac{1}{\lambda}f(\sin u; \kappa, \beta_\pm)\right], \tag{2.4}$$

with

$$f(z; \kappa, \beta_\pm) := 2\kappa^2 e^{-2\beta_+}\frac{z + \cosh(2\sqrt{3}\beta_-)}{1 - z^2} - z^2$$

$$+ 2\kappa e^{2\beta_+}[z - \cosh(2\sqrt{3}\beta_-)] - \kappa e^{-4\beta_+}. \tag{2.5}$$

Here, we have introduced the new variable κ and parameter λ as

$$\kappa := \frac{1}{12}\Lambda a^2, \quad \lambda := \frac{\hbar\Lambda}{6\pi}, \tag{2.6}$$

thereby effectively reducing the number of parameters occuring in Eq. (2.4), and we shall also make use of the variables κ_j defined by

---

[1]Here, in contrast with [I], the *total* action, including the part which affects the similarity transformation between Ashtekar and metric variables, has been defined as the exponent of the integrand.

$$\kappa_j := \kappa e^{-\beta_j}, \tag{2.7}$$

where the β_j are the entries of the diagonal anisotropy matrix $\boldsymbol{\beta}$. The integration contour $\mathcal{C}$ in the integral representation (2.4) can be chosen quite freely, as long as a sufficiently strong falloff for the integrand and its u derivatives at the borders $\partial\mathcal{C}$ of $\mathcal{C}$ is guaranteed. The proportionality factor left open in Eq. (2.4) may depend on λ and will be fixed later.

Let us now try to find a basis set of topologically independent integration contours $\mathcal{C}$. As known from [I], such a set can be constructed as follows: First one has to calculate the different saddle points of the integrand's exponent, because they obviously generate linearly independent wave functions as long as saddle point expansions of the integral representation (2.4) are considered. For any such saddle point one may now pick a curve of steepest descent of $\mathrm{Re}f/\lambda$, thereupon guaranteeing that the integrand vanishes at the end points of this curve. It is then possible to show that the ''saddle point curves'' defined in this way form a basis set of topologically independent integration contours.

While in the case $\Lambda > 0$ the curves of steepest *descent* of $\mathrm{Re}f$ were of interest, now, because of the different sign of Λ, the curves of steepest *ascent* lead to suitable integration contours. A discussion of the location of the saddle points suggests to distinguish between different regimes of the minisuperspace. To motivate our division between these different regions, let us consider the semiclassical limit $\hbar \rightarrow 0$ of the wave functions (2.4). Noticing that the only $\hbar$ dependence of Eq. (2.4) is hidden in λ via Eq. (2.6), a saddle point expansion in the limit $\hbar \rightarrow 0$ easily reveals

$$S \overset{\hbar \rightarrow 0}{\sim} -\frac{6\pi i}{\Lambda}f(z_S), \tag{2.8}$$

where z_S is the highest saddle point that must be passed through by $\mathcal{C}$. To describe a *Lorentzian* universe, the action (2.8) should have a nonvanishing real part, which is only possible for $\mathrm{Im}z_S \neq 0$. In this way the existence of complex saddle points is directly connected to the existence of wave functions which describe a Lorentzian universe. Thus, we shall subdivide the minisuperspace as follows:

(a) By choosing $|\kappa|$ sufficiently small at fixed $\beta_\pm$, it is always possible to make all five saddle points of $f(z)$ lie on the real axis of the complex z plane, defining the *Euclid I* region of minisuperspace. Note, however, that the corresponding points in the u plane of Fig. 1 (here $u = \arcsin z$) are real valued only for $|z| \leq 1$, whereas real z values with $|z| > 1$ are mapped into complex conjugate pairs of points on the axes $\mathrm{Re}u = \pm\pi/2$ and periodic repetitions thereof.

(b) Except for the case $\beta_\pm = 0$, where all five saddle points are on the real z axis, there is the possibility for two of the saddle points to become complex in the z plane, which defines the *Lorentzian regime*.

(c) For large values of $|\kappa|$ one always enters the *Euclid II* region, where again all five saddle points of $f(z)$ become real valued.

Some typical locations of the saddle points in these different regimes of minisuperspace and the corresponding curves of steepest ascent are presented in Fig. 1. By passing from one of these regions to another, a *marginal* situation

Euclid I   Lorentzian regime   Euclid II

● Saddle-point   * Singularity at $u = \pm \frac{\pi}{2}$ ⟶ $\Re f$ increases
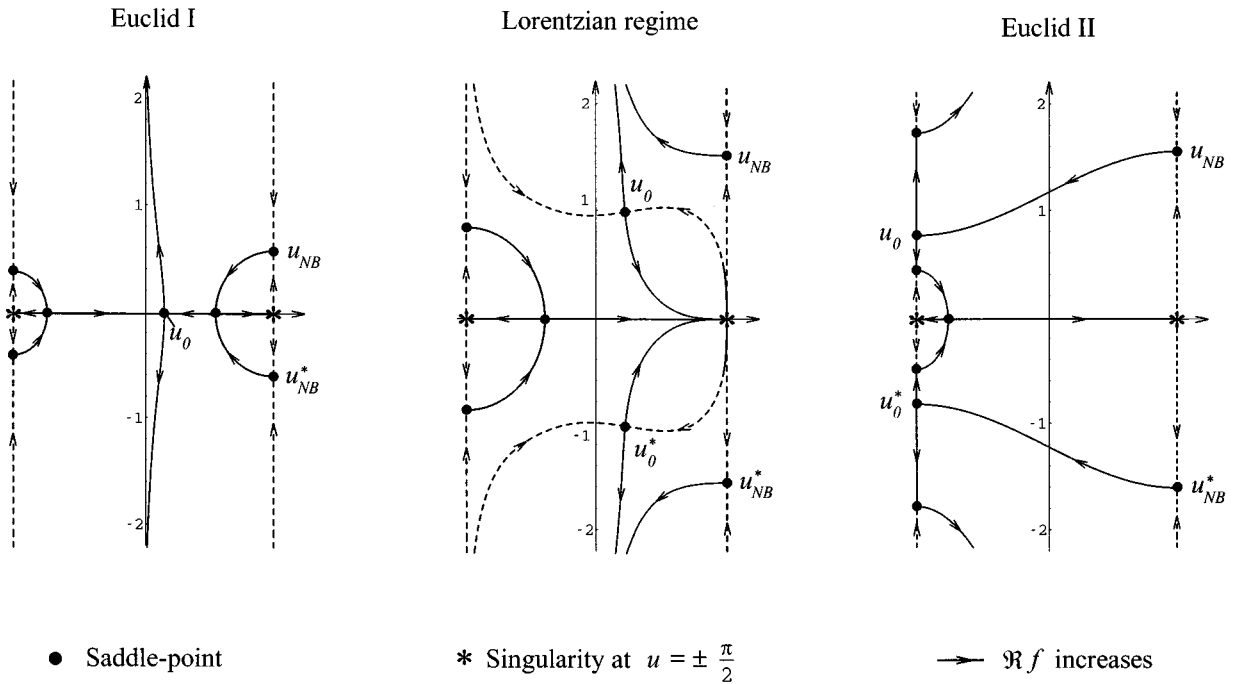
FIG. 1. Saddle points and curves of steepest ascent of $\mathrm{Re} f$ in the complex u plane for $\Lambda < 0$. The picture given in the Lorentzian case only holds for $\kappa_3 = \min\{\kappa_j\}$. The remaining case can easily be constructed by reflecting this figure on the imaginary axis. The dashed curves come from $-\infty$ with respect to $\mathrm{Re} f$ and are given just for completeness.

occurs, where two of the saddle points are confluent. We will refer to the corresponding hypersurface in minisuperspace as the *caustic*; it has been calculated and is plotted in Fig. 2. In contrast with the case $\Lambda > 0$ the caustic obtained here consists of an upper and a lower branch, which are connected just by a single *point* at $\kappa = -2$, $\beta_\pm = 0$. Furthermore, there are *kinks* at $\beta_+ > 0$, $\beta_- = 0$ and also at the other half-rays of

the $\beta_\pm$ plane, related to the former by the typical $\beta_\pm$ symmetries of diagonal Bianchi type IX.

Obviously, an exactly isotropic universe $\beta_\pm = 0$ has to stay purely Euclidean throughout its evolution. On the other hand, "large" universes with Lorentzian geometry must become very anisotropic. Apart from the possibility of a negative cosmological constant very close to zero, which would allow for large scale parameters even at $|\kappa|$ values of order one, it seems impossible for the model under investigation to describe the Universe observed today.

Nevertheless, let us now construct a basis of solutions to the Wheeler-DeWitt equation (2.3) by choosing topologically independent integration contours $\mathcal{C}$ in the representation (2.4). Using the curves defined in Fig. 3 we introduce the solutions

$$\Psi_0 := \frac{-i e^\mu}{K_0(-\mu)} \int_{\mathcal{C}_0} du \, \exp\left[\frac{1}{\lambda} f(\sin u)\right],$$

$$\Psi_\varrho := \frac{e^\mu}{\pi I_0(\mu)} \int_{\mathcal{C}_\varrho \oplus \mathcal{C}_\varrho^*} du \, \exp\left[\frac{1}{\lambda} f(\sin u)\right],$$

$$\varrho \in \{-, +, 3, NB\} \quad (2.9)$$

with

$$\mu := \frac{1}{2\lambda}, \quad (2.10)$$

FIG. 2. The caustic in minisuperspace for $\Lambda < 0$.

which, by definition, are real valued and normalized in accordance with
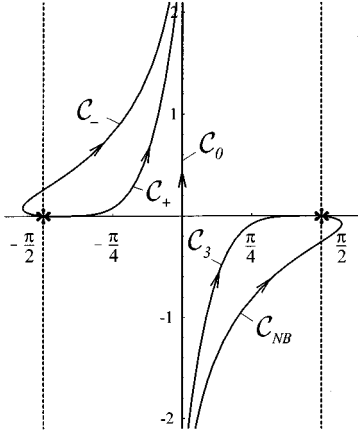
FIG. 3. Basis set of integration curves.

$$\Psi_\varrho(a=0)\equiv 1, \quad \varrho \in \{0,-,+,3,NB\}. \qquad (2.11)$$

The functions K_0 and I_0 occurring in Eq. (2.9) are the usual modified Bessel functions with index 0. To extract the asymptotic behavior of the wave functions (2.9) in a given parameter limit it is useful to deform the curves given in Fig. 3 into the curves of steepest ascent presented in Fig. 1. Clearly, this deformation of the curves depends subtly on the regime of minisuperspace and it involves some detailed topological considerations. But in the end the individual saddle point contributions to the integral are nicely displayed; in particular, the highest saddle point that must be passed through by the given integration curve is easily identified, and this is the only one which has to be taken into account when performing a saddle point expansion. In the following we only give here the *results* of the expansions obtained in this way.

It will be of some advantage to replace the solutions Ψ_+ and Ψ_- defined in Eq. (2.9) by

$$\Psi_1 := \begin{cases} \Psi_+, & \beta_- \geqslant 0, \\ \Psi_-, & \beta_- \leqslant 0, \end{cases} \quad \Psi_2 := \begin{cases} \Psi_+, & \beta_- \leqslant 0, \\ \Psi_-, & \beta_- \geqslant 0. \end{cases} \qquad (2.12)$$

Then, expansions of the integrals (2.9) in the limit $\Lambda \to 0$, a and $\beta_\pm$ fixed, reveal

$$\lim_{\Lambda \to 0} \Psi_0 = \Psi_{WH}^0, \quad \lim_{\Lambda \to 0} \Psi_{NB} = \Psi_{NB}^0,$$

$$\lim_{\Lambda \to 0} \Psi_i = \Psi_i^0, \quad i \in \{1,2,3\}, \qquad (2.13)$$

where the upper index "0" denotes the solutions of the $\Lambda = 0$ model given in [I].

We just mention that Ψ_i, $i \in \{1,2,3\}$, are three asymmetric solutions which generate each other by cyclic permutations of the κ_j, so consequently, the sum of these states,

$$\Psi_\Sigma := \frac{1}{3} \sum_{i=1}^{3} \Psi_i, \qquad (2.14)$$

in addition to Ψ_0 and Ψ_{NB}, turns out to be symmetric with respect to arbitrary κ_j permutations. An explicit proof of this

claim can be given in analogy to the case $\Lambda > 0$ detailed in [I] if the wave functions Ψ_i are replaced by the equivalent set Ψ^i defined in Eq. (2.17) below. Because of the cyclic relationship between the asymmetric states Ψ_i and the obvious nice analytical properties of Ψ_3, it is then furthermore clear that Ψ_1 and Ψ_2 defined in Eq. (2.12), in contrast with $\Psi_\pm$, are differentiable functions even at the junction $\beta_- = 0$.

Let us also consider the asymptotic behavior of the wave functions Ψ_0 and Ψ_{NB} defined in Eq. (2.9) in the limit $\kappa \to -\infty$ which finally yields

$$\Psi_0 \overset{\kappa \to -\infty}{\sim} \frac{\sqrt{\hbar}}{K_0\left(-\dfrac{3\pi}{\hbar\Lambda}\right)} \left(-\frac{3}{\Lambda}\right)^{1/4} \left(\frac{a}{2}\right)^{-3/2}$$
$$\times \exp\left[-\frac{\pi a^3}{\hbar} \sqrt{-\frac{\Lambda}{3}}\right], \qquad (2.15)$$

$$\Psi_{NB} \overset{\kappa \to -\infty}{\sim} \frac{\sqrt{\hbar}}{\pi I_0\left(\dfrac{3\pi}{\hbar\Lambda}\right)} \left(-\frac{3}{\Lambda}\right)^{1/4} \left(\frac{a}{2}\right)^{-3/2}$$
$$\times \exp\left[+\frac{\pi a^3}{\hbar} \sqrt{-\frac{\Lambda}{3}}\right], \qquad (2.16)$$

at $\beta_\pm = 0$, i.e., while Ψ_0 falls off rapidly for $a \to \infty$, the wave function Ψ_{NB} is strongly divergent in the same limit. Moreover, since Ψ_{NB} *always* gets its dominant contribution from the real saddle point $z \geqslant 1$ (corresponding to the points u_{NB} and u_{NB}^* in the complex u plane of Fig. 1 via $z = \sin u$), just Euclidean geometries are described by this state, so we will reject Ψ_{NB} as a physically relevant solution. Note, however, that it is the only state which satisfies the *no-boundary* condition in the limit $\hbar \to 0$, $a \to 0$; hence, the name of this wave function.

To give the asymptotic behavior in the limit $\kappa \to -\infty$ for the states Ψ_i, $i \in \{1,2,3\}$, it will be helpful to consider

$$\Psi^i := \frac{1}{2}(\Psi_j + \Psi_k), \quad \varepsilon_{ijk} = 1 \qquad (2.17)$$

instead. For these solutions the asymptotic expansions

$$\Psi^i \overset{\kappa \to -\infty}{\sim} -\frac{\Psi_{WH}^0}{I_0(\mu)} \sqrt{-\frac{\lambda}{\pi}} \frac{2}{\kappa_i} \left\{ 1 - 2\frac{\kappa_j \kappa_k}{\kappa_i^3} \right\}$$
$$\times \exp\left[\frac{1}{\lambda}\left(\kappa_i^2 - 2\frac{\kappa_j \kappa_k}{\kappa_i}\right)\right], \quad \varepsilon_{ijk} = 1 \qquad (2.18)$$

hold, so they fall off very rapidly for $a \to \infty$ (remember the negative sign of λ).

By considering additional asymptotic expansions for large anisotropy it is possible to show that the four states Ψ_i, $i \in \{0,1,2,3\}$ are all normalizable on minisuperspace in the distribution sense (see [I] for a discussion of this point for $\Lambda > 0$), i.e., so far we are left with a still four-dimensional space of physically interesting solutions.

However, while in the Lorentzian regime Ψ_0 receives saddle point contributions exclusively from the saddle points at *complex z* and thus describes a Lorentzian universe in this
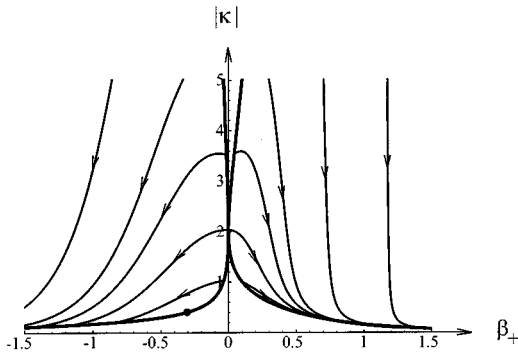
FIG. 4. Semiclassical trajectories generated by the complex saddle points in the Lorentzian regime. For simplicity, we have restricted the plot to the plane $\beta_- = 0$. The arrows indicate the direction of increasing time t in Eq. (2.19).

part of minisuperspace, the states Ψ_i, $i \in \{1,2,3\}$ in addition also get Euclidean contributions of similar order of magnitude from *real* saddle points and are, therefore, hard to interpret. For a discussion of the semiclassical behavior we shall, therefore, restrict ourselves to the wave function Ψ_0. Taking account of Eq. (2.8), the Lorentzian, classical trajectories in the limit $\hbar \to 0$ may be calculated by solving the equations

$$\frac{d\alpha}{dt} = -\frac{d\,\mathrm{Im}f(z_0)}{d\alpha}, \quad \frac{d\beta_{\pm}}{dt} = \frac{d\,\mathrm{Im}f(z_0)}{d\beta_{\pm}}, \quad (2.19)$$

where we have chosen the lapse function to be $N = \frac{1}{2}\Lambda a^3$. While the complex saddle point z_0 occurring in Eq. (2.19) is intended to correspond to the point u_0 of Fig. 1, its complex conjugate counterpart $z_0^* = \sin u_0^*$, which describes the time-reversed classical evolution, can be considered with the same justification. The corresponding second branch of the classical evolution of the Universe is actually necessary to define the continuation of a classical trajectory which has reached the caustic: in approaching the caustic the saddle points z_0 and z_0^* become confluent and real valued, so that, in accordance with Eq. (2.19), the time derivatives of α and $\beta_{\pm}$ vanish. To continue such a trajectory in time, the time-reversed version of Eq. (2.19) has to be considered. Since the Universe is ''reflected'' in this way whenever it meets the caustic, and since in the generic case the classical trajectories have both of their end points on the caustic, *oscillating* universes are described by Ψ_0.

The numerical results for the classical trajectories which are obtained in the plane $\beta_- = 0$ of the minisuperspace are presented in Fig. 4. We should stress one important difference obtained for the different signs of β_+. While for $\beta_+ > 0$, $\beta_- = 0$ all trajectories run to infinite anisotropy (which is, indeed, a peculiarity of the special $\beta_{\pm}$ direction, corresponding to a kink on the caustic, cf. Fig. 2), in the case $\beta_+ < 0$ the trajectories meet the lower branch of the caustic again at a finite β_+ value, representing the general situation. This feature gives rise to the existence of a special trajectory, represented by a dot in Fig. 4, with coinciding start and end points; hence, describing a universe that never becomes Lorentzian. The corresponding points in minisuperspace can

be calculated analytically, requiring the solution of Eq. (2.19) to be *tangential* to the caustic, with the result

$$\kappa = -\sqrt[3]{2}\left(\frac{2}{5}\right)^{4/3}, \quad \beta_+ + i\beta_- = \frac{1}{6}(\ln 5 - 5\ln 2)e^{2\pi in/3},$$

$$n \in \{-1,0,1\}. \quad (2.20)$$

These points will play an important role in the following section.

III. BEHAVIOR ON THE CAUSTIC

Since the classical Lorentzian evolution of the universe described by the wave functions Ψ_i, $i \in \{0,1,2,3\}$, is bounded by the caustic in minisuperspace, the value of $|\Psi|_c^2$ *on the caustic* predicted by the different solutions is of particular interest. In fact, $|\Psi|_c^2$ governs the realization of the different possible histories of the universe and may thus be interpreted as the ''initial'' value distribution for the classical evolution.

However, at this stage a new problem arises because of the different branches of the caustic. Since the semiclassical trajectories always can be passed through in both directions, it is impossible to distinguish between their start and end points. The distributions of $|\Psi|_c^2$ on the upper and lower branches of the caustic may, therefore, be considered with the same justification, and we will always discuss them together in the following.

The numerical results obtained for $|\Psi_0|_c^2$ and $|\Psi_\Sigma|_c^2$ on the lower caustic are given in Fig. 5, while Fig. 6 shows the behavior on the upper caustic, which is very similar for the two different solutions. In the following the additional indices ''u'' and ''l'' denote the upper and lower branch of the caustic, respectively. While on the upper caustic both distributions fall off rapidly with increasing $\beta_{\pm}$ and may be shown to be integrable over the $\beta_{\pm}$ plane, there are $\beta_{\pm}$ directions on the lower caustic, in which $|\Psi|_{c,l}^2$ approaches a finite value at infinity. Consequently, the wave functions on the lower branch are *not* square integrable and, hence, difficult to interpret as probability distributions. Nevertheless, as in the case $\Lambda > 0$, one may construct a new wave function as a linear combination of the two symmetric wave functions Ψ_0 and Ψ_Σ: By normalizing Ψ_0 and Ψ_Σ to approach unity in the critical $\beta_{\pm}$ directions, the difference of these new functions is square integrable on the *full* caustic. To give an explicit expression for the quantum state obtained in this way, we introduce the integrals

$$\mathcal{J}_0^{(1)}(\nu) := \int_{-\pi/4}^{+\pi/4} dx \, e^{-\nu \sin^4 x},$$

$$\mathcal{J}_0^{(2)}(\nu) := \int_{-\pi/4}^{+\pi/4} dx \, e^{-\nu \cos^4 x},$$

$$\mathcal{K}_0^{(1)}(\mu) := \int_0^{\infty} dx \, \sin(4\mu \, \sinh t)e^{\mu \cosh 2t},$$

$$\mathcal{K}_0^{(2)}(\mu) := \int_0^{\infty} dx \, \cos(4\mu \, \sinh t)e^{\mu \cosh 2t}, \quad (3.1)$$

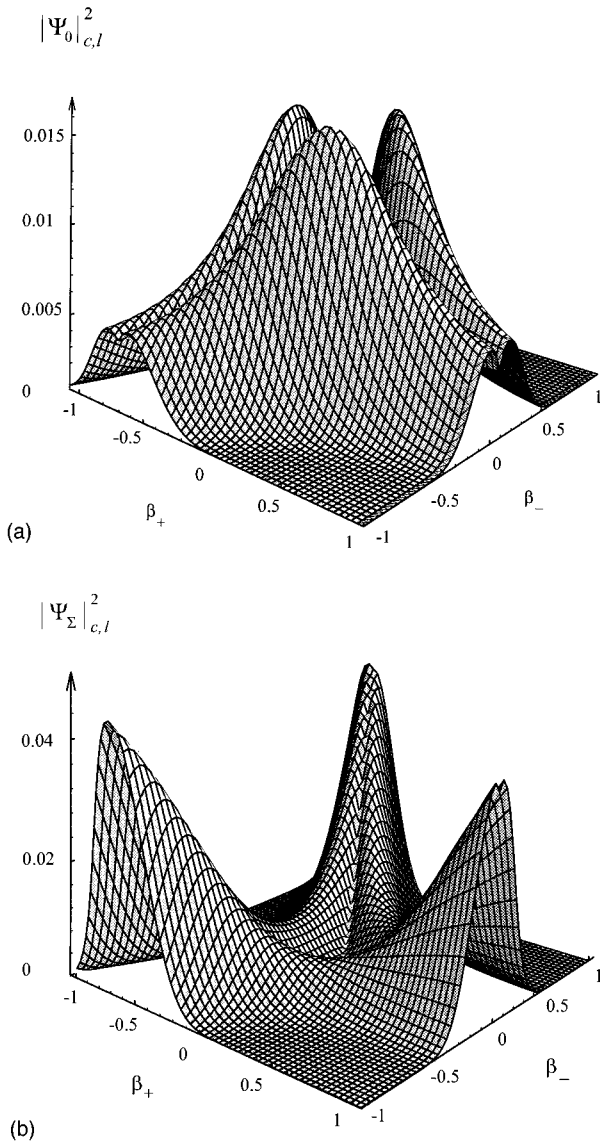which, as far as we know, have no simple representation in terms of tabulated functions. Defining now

$|\Psi_0|^2_{c,l}$

(a)

$|\Psi_\Sigma|^2_{c,l}$

(b)

FIG. 5. Initial value distributions generated by Ψ_0 and Ψ_Σ on the lower caustic ($\Lambda=-3$, $\hbar=2\pi$). Like the caustic itself, the distributions have kinks in some critical $\beta_\pm$ directions, which are partially hidden in the figures.

$$\mathcal{Q}(\lambda):=3\pi e^{-3\mu}\frac{I_0(\mu)}{K_0(-\mu)}$$

$$\times\frac{\mathcal{K}_0^{(2)}(\mu)}{2\mathcal{J}_0^{(1)}(8\mu)+\mathcal{J}_0^{(2)}(8\mu)+e^{-3\mu}\mathcal{K}_0^{(1)}(\mu)},$$

$$\text{with } \mu=\frac{1}{2\lambda}, \quad (3.2)$$

the new state can be written in the form

$$\hat{\Psi}:=\frac{\Psi_0-\mathcal{Q}\Psi_\Sigma}{1-\mathcal{Q}}, \quad (3.3)$$

where the overall normalization factor has again been chosen to make $\hat{\Psi}\equiv1$ at $a=0$. The behavior of $\hat{\Psi}$ on the caustic has been computed for Fig. 7. Taking account of the full distri-
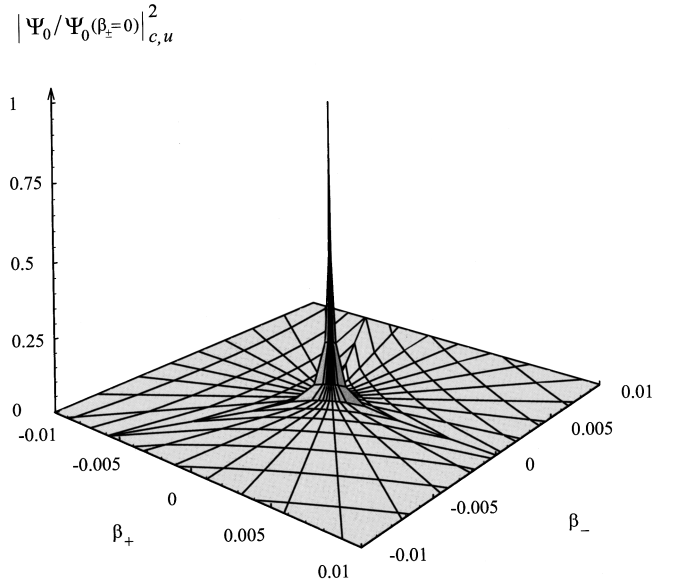
$|\Psi_0/\Psi_{0(\beta_\pm=0)}|^2_{c,u}$

FIG. 6. Initial value distribution of Ψ_0 on the upper caustic, normalized to unity at $\beta_\pm=0$. The numerical plots obtained for the different wave functions Ψ_0 and Ψ_Σ (and thus for $\hat{\Psi}$ defined below) on the upper caustic look very similar, so we restrict ourselves to a representation of $|\Psi_0|^2_{c,u}$. The absolute values taken by $|\Psi|^2_{c,u}$ at $\beta_\pm=0$ are given by 1.45×10^{-11}, 3.56×10^{-13}, and 2.43×10^{-11} for the wave functions Ψ_0, Ψ_Σ, and $\hat{\Psi}$, respectively (here again, $\Lambda=-3$, $\hbar=2\pi$). Since the lower and upper caustic coincide at $\beta_\pm=0$, it is clear that these values hold for the distributions on the lower caustic, too. That is why we suggest to consider the two distributions obtained on the different branches of the caustic as analytical continuations of each other through the isotropic point.

bution, three maxima on the lower branch of the caustic pick out special initial values for the classical evolution of the Universe. The general representation (2.4) easily reveals that the wave function becomes arbitrarily sharply concentrated about these maxima in the limit $\lambda\to0$, i.e., in particular in the limit $\hbar\to0$ at fixed Λ. Consequently, in the semiclassical limit there are just three histories of the Universe which occur with significant probability.

In the following we shall be interested in the special points of minisuperspace where the maxima of $|\hat{\Psi}|^2_{c,l}$ arise. Using the saddle point method for $\lambda\to0$ the asymptotic behavior of the integrals defined in Eq. (3.1) after some calculation yields

$$\mathcal{Q}\overset{\lambda\to0}{\sim}\frac{3}{2}\sqrt{\frac{2}{\pi}}\Gamma(\tfrac{1}{4})(-\lambda)^{-1/4}e^{3/\lambda}, \quad (3.4)$$

and with this result the relation

$$\hat{\Psi}\overset{\hbar\to0}{\sim}\Psi_0 \quad (3.5)$$

can be shown to hold at least on the lower caustic. Since $\hat{\Psi}$ is a real valued, nonvanishing wave function, the maxima of $|\hat{\Psi}|^2$ coincide with the maxima of $\hat{\Psi}$, and using Eq. (3.5) they may also be calculated from Ψ_0 in the semiclassical limit. By performing again a saddle point expansion for $\lambda\to0$, now in the integral representation Eq. (2.9) of Ψ_0, the

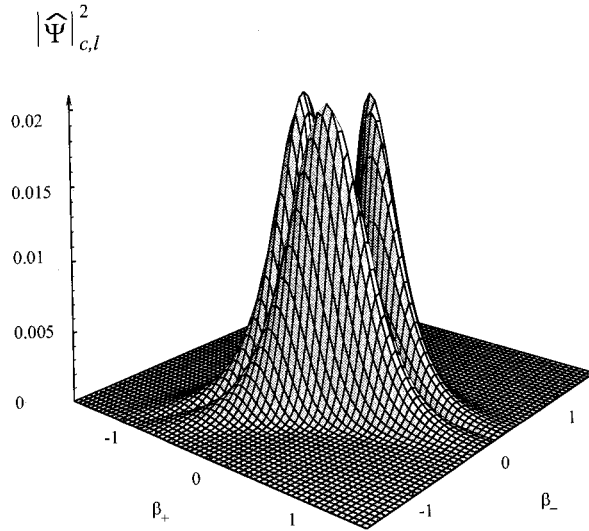FIG. 7. Initial value distribution generated by $\hat{\Psi}$ on the lower caustic ($\Lambda = -3$, $\hbar = 2\pi$). For the distribution obtained on the upper caustic see Fig. 6.

maxima of Ψ_0 on the caustic can be calculated analytically with the result given exactly by Eq. (2.20).

Consequently, within the class of solutions considered here, the *only* quantum state that is square integrable on the full caustic turns out to predict a universe which never becomes Lorentzian in the classical limit (albeit classical Lorentzian solutions of the Bianchi type IX model with negative cosmological constant actually do exist, cf. Fig. 4).

IV. CONCLUSION

In the present paper we constructed exact quantum states for the diagonal Bianchi type IX model with a negative cosmological constant. We found that the method presented in [I] for $\Lambda > 0$ is indeed perfectly applicable to the model with $\Lambda < 0$. As for $\Lambda > 0$ it gives five linearly independent solutions, which are generated by the Chern-Simons state using topologically different integration contours in the generalized Fourier transformation to the metric representation. Provided the square integrability of the wave function on the caustic surface in minisuperspace is accepted as an essential condition (and this is the point of view we have adopted throughout this paper), just one wave function remains that turns out to have some nice additional properties: It is found to be normalizable in minisuperspace in the distribution sense and it respects the symmetries of the Bianchi type IX model. However, this state does *not* satisfy the no-boundary condition in the semiclassical limit in contrast with the case $\Lambda > 0$, and it turns out to predict a universe that never becomes Lorentzian, after all. Hence, we obtain the result that, *if* one allows for a nonzero cosmological constant at all, it should be positive, at least as far as the Chern-Simons functional-related states of the quantized Bianchi type IX model are concerned.

APPENDIX: SOLUTIONS IN A DIFFERENT FACTOR ORDERING

For completeness, and in order to obtain an important argument for the factor ordering chosen for the Wheeler-DeWitt equation (2.3), we shall make some comments on a further class of solutions, which can again be discussed by using the methods of [I].

Considering the Wheeler-DeWitt equation in the form (2.1), one may ask why we have not chosen a different factor ordering, which is obtained by changing $\Phi \rightarrow -\Phi$. This choice, of course, would not have affected the classical Hamiltonian, but the quantum correction $-(2\hbar/\pi)a^2 \mathrm{Tr} e^{2\beta}$ in Eq. (2.3) would have changed its sign.[2] Since the coordinate transformation $a \rightarrow ia$, $\Lambda \rightarrow -\Lambda$ has exactly the same effect as the above-mentioned change of the factor ordering, it is possible to discuss the solutions of the Wheeler-DeWitt equation in the new factor ordering by considering still Eq. (2.3), but substituting formally $a \rightarrow ia$, $\Lambda \rightarrow -\Lambda$ in the solutions. In the following it will be more convenient to use the coordinates κ_j and λ introduced in Eqs. (2.6) and (2.7), which transform such as $\kappa_j \rightarrow \kappa_j$, $\lambda \rightarrow -\lambda$ under this substitution.

It should be clear that the solutions of the Wheeler-DeWitt equation (2.3) are still of the form (2.4), but while we looked at the cases $\kappa > 0$, $\lambda > 0$ in [I] and $\kappa < 0$, $\lambda < 0$ in the present paper, now the remaining sectors $\kappa > 0$, $\lambda < 0$ and $\kappa < 0$, $\lambda > 0$ are of interest which, because of the formal substitution $\lambda \rightarrow -\lambda$ just mentioned, describe solutions for *positive* and *negative* cosmological constant in the *new* factor ordering, respectively. It is easily checked that the location of the saddle points and, therefore, the caustic, depends only on $f(z;\kappa,\beta_\pm)$ defined in Eq. (2.5). This means that, irrespective of the sign of λ, we deal with the caustic of [I] in the case $\kappa > 0$, and with the caustic of Fig. 2 in the case $\kappa < 0$. On the other hand, it is just the sign of λ which decides whether the integration curves of [I] (for $\lambda > 0$) or of Fig. 3 (for $\lambda < 0$) give suitable integration contours.

However, constructing the solutions for the new factor ordering in this manner and applying the saddle point method to the integral representation (2.4) in the limit of large anisotropy $\beta_\pm$, it finally turns out that *any* solution to the Wheeler-DeWitt equation in the new factor ordering *diverges* for $\beta_\pm \rightarrow \infty$, at least in some $\beta_\pm$ sectors. In other words, in the new factor ordering there is no solution which is normalizable in minisuperspace, not even in the distribution sense. Furthermore, if the behavior of the wave func-

---

[2]The factor ordering obtained in this way corresponds to the $\mathcal{A}^+$ representation introduced by Kodama in [6], in contrast with the $\mathcal{A}^-$ representation, which we have considered up to now.

tions on the caustic is considered, actually none of these solutions is found to be square integrable with respect to $\beta_\pm$.

Comparing these results with the nice normalizability properties of the solutions of the Wheeler-DeWitt equation in the factor ordering of Eq. (2.1) presented in [I] and the present paper, we believe to have a compelling argument to rule out the new factor ordering. It would be interesting if this argument could be extended even to the general, inhomogeneous case of quantum gravity.

---

[1] A. Ashtekar, Phys. Rev. Lett. **57**, 2244 (1986); Phys. Rev. D **36**, 295 (1987).

[2] A. Ashtekar, in *Lectures on Nonperturbative Canonical Gravity* (World Scientific, Singapore, 1991).

[3] A. Ashtekar, in ''Polymer Geometry at the Planck Scale and the Quantum Einstein Equations,'' Report No. hep-th/9601054 (unpublished).

[4] C. J. Isham, ''Structural Issues in Quantum Gravity,'' Report No. gr-qc/9510063 (unpublished).

[5] K. Ezawa, ''Nonperturbative solutions for canonical quantum gravity: an overview,'' Report No. gr-qc/9601050 (unpublished).

[6] H. Kodama, Phys. Rev. D **42**, 2548 (1990).

[7] M. P. Brencowe, Nucl. Phys. **B341**, 213 (1990).

[8] R. Graham and R. Paternoga, Phys. Rev. D **54**, 2589 (1996). This paper is quoted as [I].

[9] J.B. Hartle and S.W. Hawking, Phys. Rev. D **28**, 2960 (1983).

[10] S.W. Hawking, Nucl. Phys. **B239**, 257 (1984).

[11] W. Freedman *et al.*, Nature (London) **371**, 757 (1994).

[12] R. Graham, Phys. Rev. Lett. **67**, 1381 (1991).

[13] J. Bene and R. Graham, Phys. Rev. D **49**, 799 (1994).

[14] A. Csordás and R. Graham, Phys. Rev. Lett. **74**, 4129 (1995).